Electrochimica Acta 497 (2024) 144533

Contents lists available at ScienceDirect

Electrochimica Acta

journal homepage: www.journals.elsevier.com/electrochimica-acta

Advancing hydrogen peroxide electro-generation: Selective production at high rates in a flow-through module

Mojtaba Mohseni [a,1], Waralee Dilokekunakul [a,1], Matthias Wessling [a,b], Robert G. Keller [a,*]

[a] RWTH Aachen University, Aachener Verfahrenstechnik - Chemical Process Engineering, Forckenbeckstr. 51, 52074 Aachen, Germany
[b] DWI - Leibniz Institute for Interactive Materials, Forckenbeckstr. 50, 52074 Aachen, Germany

ARTICLE INFO

Keywords:
Carbon black catalysts
Electro-generation of hydrogen peroxide
Hetero-atom doped carbons
Flow-through reactors
High current densities

ABSTRACT

Electrochemical synthesis of hydrogen peroxide (H_2O_2) via oxygen reduction reactions (ORR) represents a green, environmentally friendly, and decentralized alternative to the conventional, fossil-based, and centralized anthraquinone process. This work presents a flow-through module using commercial carbon black (CB) as a catalyst at current densities of up to 120 mA cm^{-2}. Acid treatment of CB increases its oxygen content, leading to Faraday efficiency (FE) values above 80 % with a maximum specific H_2O_2 production rate of 64.3 mg cm^{-2} h^{-1}. Additionally, the effect of catalyst loading on the functionality of a gas diffusion electrode (GDE) at 120 mA cm^{-2} and over long-term electrolysis (7.5 h) is investigated, discussing the detrimental penetration of electrolyte into the GDE due to the enhanced electro-wetting, which shifts the three-phase boundary toward the gas channel side. This study underscores the critical significance of optimizing the parameters involved in GDE fabrication, especially under high current densities and extended operational periods, propelling our understanding toward the development of a robust flow-through module for the electro-generation of H_2O_2.

1. Introduction

Hydrogen peroxide (H_2O_2) is gaining recognition in green chemistry due to its eco-friendliness and various uses. Its decomposition into harmless water and oxygen makes it a "green" oxidant and reagent. Predominantly produced through the anthraquinone process, H_2O_2 plays a vital role in chemical industries, valued for its efficiency and cost-effectiveness [1,2]. It also contributes to healthcare and sanitation as a powerful disinfectant, notably effective against pathogens like SARS-CoV-2 [3,4]. In industrial sectors, H_2O_2 is an oxidizing agent for textile bleaching, paper production, wastewater treatment, and rocket propulsion, attributing to its environmental compatibility [5,6]. As a mild oxidizing agent in chemical reactions, it facilitates selective organic transformations. The combination of its versatility and minimal environmental impact highlights H_2O_2's pivotal role in advancing sustainable and green chemical practices, with an annual market production nearing 3000 kt (4.57 billion USD in 2023) [7,8].

Currently, approximately 95% of H_2O_2 is manufactured using the indirect anthraquinone process [9]. Despite the high efficiency of the anthraquinone process and obtaining H_2O_2 concentrations up to 70 wt%, this process requires complex and costly infrastructure, meticulous maintenance, precise monitoring due to the use of hazardous materials, and environmental impacts because of periodic catalyst replacements. Alternatively, hydrogen peroxide (H_2O_2) can also be synthesized directly from hydrogen (H_2) and oxygen (O_2) at low temperatures using palladium-based catalysts, which enables a continuous and decentralized process. [10–12]. However, the potential risk of forming an explosive mixture of oxyhydrogen (H_2 + O_2) in the direct synthesis process presents a challenge to its application in decentralized H_2O_2 production units.

On the other hand, required concentrations of H_2O_2 at the use points are, in practice, significantly lower. For instance, a concentration as low as 0.4 wt% and lower than 6 wt% is sufficient for water treatment and antimicrobial purposes, respectively [13,14]. Therefore, highly concentrated (>27 wt%) H_2O_2 solutions are produced and transported from centralized units to end-users, where H_2O_2 is stored and diluted before usage, which is costly and hazardous [15–18].

A paradigm shift in H_2O_2 synthesis is its electrochemical synthesis through the two-electron oxygen reduction reaction (ORR) [19–27]. Research in catalysis has pursued the development of non-precious catalysts with ORR activity similar to platinum (Pt). Materials like chalcogenides, transition metal compounds, carbides, and nitrides have emerged as alternatives. Notably, chalcogenides like Ru_xSe_y have gained attention. Despite platinum being the most active catalyst, its cost and availability issues have led to an interest in non-precious

* Corresponding author.
E-mail address: manuscripts.cvt@avt.rwth-aachen.de (R. Keller).
[1] These authors contributed equally to this work.

https://doi.org/10.1016/j.electacta.2024.144533
Received 30 January 2024; Received in revised form 22 April 2024; Accepted 2 June 2024
Available online 3 June 2024

carbon-based alternatives for ORR catalysis [28–30]. Carbon catalysts have been widely used for electro-generation of H_2O_2 due to their cost-effectiveness, large surface areas, their versatility in doping and modification with different functional groups, and their selectivity [31–37]. Specifically, carbon blacks such as Printex L6 and Vulcan 72R have been extensively employed in various applications owing to their high surface area and electrical conductivity [38]. In the context of the electro-generation of hydrogen peroxide or other electrochemical processes, these carbon blacks serve as catalyst supports or components of gas diffusion electrodes, thereby facilitating mass transport and electrochemical activity [38–41]. Synthesizing carbon catalysts for electro-generation of H_2O_2 has been widely studied, reporting specific H_2O_2 production rates from $6.8\,mg\,cm^{-2}\,h^{-1}$ to $23.6\,mg\,cm^{-2}\,h^{-1}$ with selectivities up to 87% [42–58]. However, synthesizing new catalysts commonly requires several delicate steps that cannot be facilely scaled up [50–53].

Additionally, these studies usually focus on the short-term (<2 h) behavior of catalysts through screening beaker experiments using small electrode areas, e.g., $<4\,cm^2$ and low current densities ($<50\,mA\,cm^{-2}$) [42–45,54,55,59]. Therefore, understanding H_2O_2 electrosynthesis over long-term experiments (>5 h) at current densities above $100\,mA\,cm^{-2}$ using larger electrode's areas ($>4\,cm^2$) in a flow-through module is fairly limited [58]. Most of the studies focusing on the electro-generation of H_2O_2 at high current densities ($>100\,mA\,cm^{-2}$) deployed electrode areas between $1\,cm^2$ to $4\,cm^2$ [53,56,59], which cannot properly reflect the impact of scaling-up on the behavior of the electrode at industry-relevant current densities.This is particularly crucial for the electro-generation of H_2O_2 since a gas diffusion electrode (GDE) must be deployed as the heart of the production unit, particularly for industrial-scale H_2O_2 generation [60].

Although a GDE provides a three-phase boundary and enhances the mass transport of sparingly soluble gaseous reactants, e.g., O_2, it suffers from flooding that usually occurs at longer electrolysis times. Flooding or undesired electrolyte ingress into the GDE shifts the location of the three-phase boundary toward the gas channel, causing complete wetness of the catalyst layer and electrolyte loss into the gas channel, which is particularly crucial for liquid products such as H_2O_2 [61].

This work presents a flow-through module for the electro-generation of H_2O_2 using acid-modified commercial carbon black catalysts at current densities up to $120\,mA\,cm^{-2}$, aiming at accelerating the transition phase from catalyst development to real-life experimental conditions. Besides the characterization of as-modified CB catalysts, their functionality and selectivity for electro-generation H_2O_2 are demonstrated. Additionally, GDEs with different catalyst loading are investigated before and after short- (60 min) and long-term (450 min) experiments, highlighting the change in wettability over time and its influence on the efficiency of the whole process.

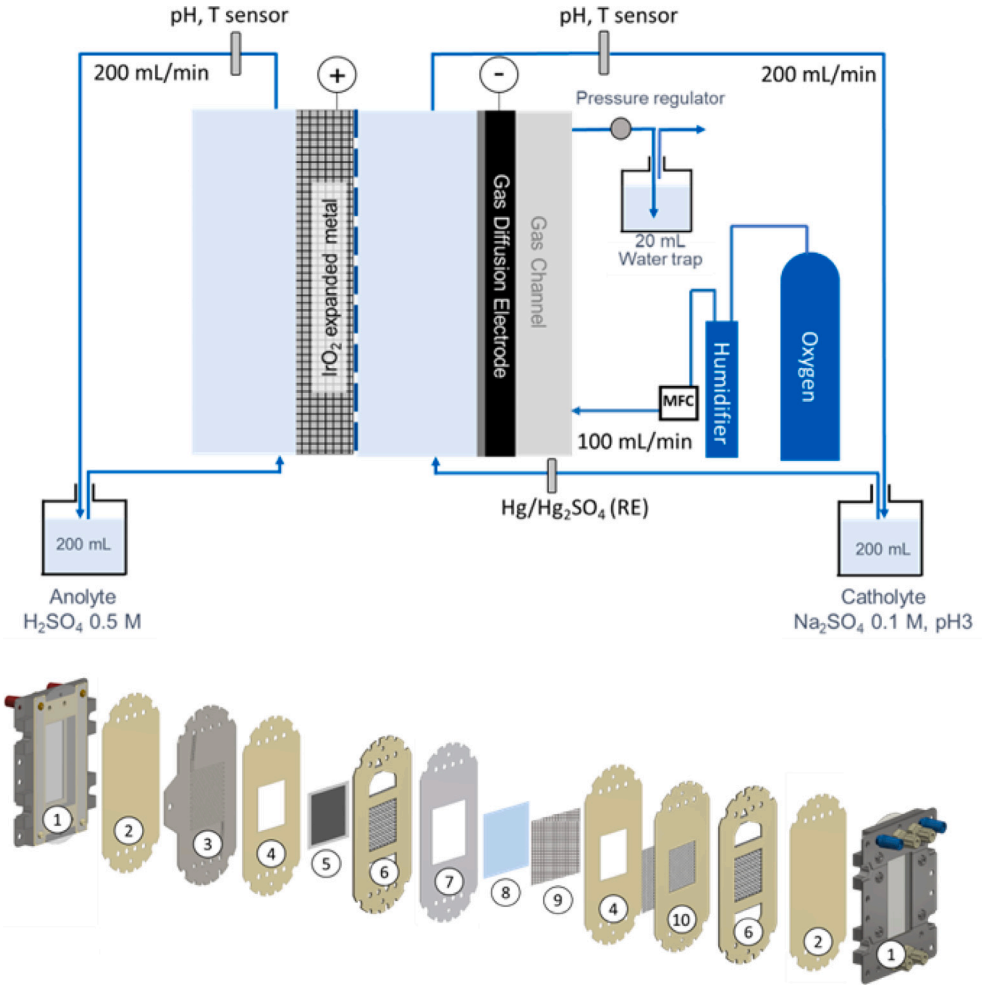

Fig. 1. Schematic diagram of experimental setup (Top) and flow-cell assembly, the number representing as follows (1) Cell housing, (2) Sealing layer, (3) Meander gas flow frame, (4) Electrode frame, (5) Gas diffusion electrode (Cathode), (6) Liquid flow frame, (7) Membrane frame, (8) Cation exchange membrane (Nafion117), (9) IrO_2 expanded metal (Anode) and (10) Current collector (Bottom).

2. Materials and methods

2.1. Materials

Ammonium metavanadate (NH_4VO_3), 30% H_2O_2, and sodium sulfate (Na_2SO_4) were purchased from Sigma-Aldrich. Gas diffusion layers (GDL340), made of carbon paper coated with a microporous layer, and 20 wt% nafion solution were provided by Quintech. Gaseous oxygen (O_2, 99.995 %), Nitric acid (HNO_3, 69 wt%), and sulfuric acid (H_2SO_4, 0.5 M) was bought from Nippon gases, Sulpeco, and VWR Chemicals, respectively. Commercial carbon black powders (VULCAN XC72R) with an average particle size of 50 nm were purchased from Cabot.

2.2. Carbon acid treatment and characterization

Acid treatment of commercial carbon black (CB) was conducted by baking 500 mg CB at 85 °C in a 12 M nitric acid solution for 1 h, 2 h, 4 h, and 7.5 h residence time. Afterward, the slurry solution was filtered and washed with deionized water and ethanol until a neutral pH was obtained, followed by a drying step at 60° under vacuum conditions 75 mbar (Fig.S1A). Based on their residence time, the acid-treated samples are designated as CB-1h, CB-2h, CB-4h, and CB-7.5h. CB-0h represents as-received CB catalysts without any acid treatment. As-prepared catalysts were then characterized by elemental analysis (EA) of the bulk phase using the Vario EL cube model (Elementar Corporation). All samples were measured twice for elemental analysis. Surface functional group analysis was carried out using X-ray photoelectron spectroscopy (XPS) with an Ultra Axis TM spectrometer from Kratos Analytica. As-synthesized CB catalysts were analyzed by the N_2-physisorption technique at 77 K using ASAP2020, micrometrics. All samples were degassed under vacuum at 250 °C for 24 h before measurement. The pore size distribution and specific surface area are computed based on the density functional theory (DFT) and Brunauer–Emmett–Teller (BET) model, respectively, which is recommended for micro- and mesoporous materials [62].

2.3. Electrode fabrication and characterization

For preparing GDEs, a catalyst ink consisting of Nafion (20 wt%), isopropanol, and as-prepared CBs was prepared with a CB: Nafion ratio of 5:1. The ink was sonicated (GT-7810A, Globaltronic) for 30 min before airbrushing. Using an airbrushing technique (Harder&Steinbeck, Evolution Silverline), The catalyst ink was evenly applied onto a Gas Diffusion Layer (GDL340, Quintech) serving as the substrate, which includes a microporous layer (MPL). After spraying, catalyst-coated GDLs were thermally treated at 130 °C for 1 h. Fig.S1B depicts a schematic representation of GDE fabrication steps. Catalyst loading was determined by weighing GDL before and after airbrushing. A catalyst loading of 0.46 mg cm^{-2} was applied unless otherwise mentioned.

Fabricated GDEs were characterized by Field Emission Electron Microscopy (FESEM) and Energy-Dispersive X-ray Spectroscopy (EDX) using a Hitachi SU5000 to visualize the distribution of the catalyst layer and its thickness and to identify its composition, respectively. Fourier-transform infrared spectroscopy (FTIR) technique was also used to qualitatively identify functional groups of the fresh and used electrodes (Perkin Elmer, LAS 60000 400695). Additionally, The degree of hydrophobicity or hydrophilicity of GDEs was determined by measuring the contact angle (KRÜSS) of a water droplet (containing 0.1 M Na_2SO_4) on their surface, measuring the angle formed between the tangent of the drop and the solid surface (GDE). Surfaces with a contact angle below and above 90° are considered hydrophilic and hydrophobic, respectively.

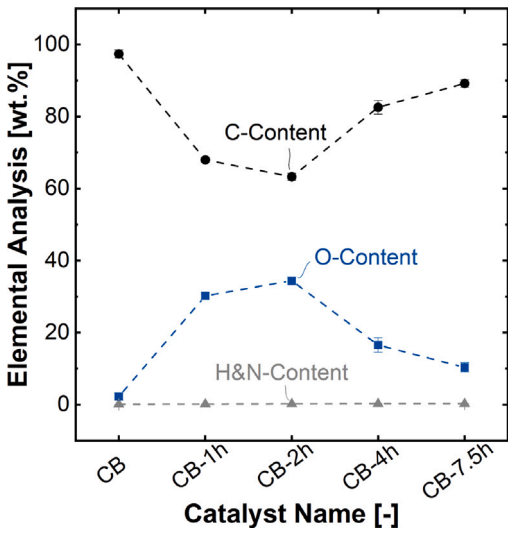

Fig. 2. Elemental analysis of as-prepared CB catalysts measured as duplicates. Each point represents the average value with standard deviation as error bars.

2.4. Electro-generation of H_2O_2

Electrolysis experiments were conducted in a three-electrode setup using a Flex-E-Cell (Flex-X-Cell GmbH). As-fabricated GDEs (6 cm × 6 cm) and Iridium(IV)-oxide expanded metal (Umicore, Ti-support, 6 cm × 6 cm) with an active geometrical surface area of 25 cm^2 served as cathode and anode, respectively; while a potassium saturated Hg/Hg_2SO_4 (0.64 V vs. SHE) was used as a reference electrode at the catholyte's inlet stream (Fig. 1C). The electrodes were connected to a potentiostat (SP-150, Biologic) for constant current experiments. 200 mL (unless otherwise mentioned) of 0.5 M H_2SO_4 and 0.1 M of Na_2SO_4 was circulated at a flow rate of 200 mL min^{-1} as anolyte and catholyte, respectively. Oxygen was supplied on the back of GDEs with a flow rate of 100 mL min^{-1} using an Alicat gas flow meter (MC-5 SLPM-D). The outlet of the oxygen gas was directed to a water trap (20 mL DI water), and a back pressure valve (Swagelok) was deployed for pressure control. Additionally, the pH and temperature of the electrolytes were monitored during electrolysis by a pH meter (Knick SE555) connected to a control unit (ZUMOLab GmbH, Wesseling, Germany).

2.5. Analytical methods

The concentration of H_2O_2 at certain time intervals was determined using a colorimetric method at 450 nm through the formation of peroxovanadium cations [63]. The concentration of sodium ions in water trap collected from the backside of GDEs was determined using ion chromatography (Compact 930 IC Flex, Metrohm) equipped with a conductivity sensor.

3. Results and discussion

3.1. Characterization of catalysts and GDEs

Functionalization of carbon catalysts with oxygen-containing groups, e.g., ethers (C−O−C) and carboxylic acids (HO−C=O), have shown selectivity toward H_2O_2 electro-generation [25,53,57]. Fig. 2 depicts the oxygen (O), carbon (C), hydrogen (H), and nitrogen (N) content detected by elemental analysis for CBs with different acid-treatment residence time. Accordingly, as-received CB contains 97.4 ± 1.1 wt% carbon with 2.2 ± 1.0 wt% O. Acid treatment leads to an increase in O content to 30.2 ± 0.8 wt% and 34.4 ± 1.1 wt% for 1 h (CB-1h), 2 h (CB-2h), respectively, which is in agreement with

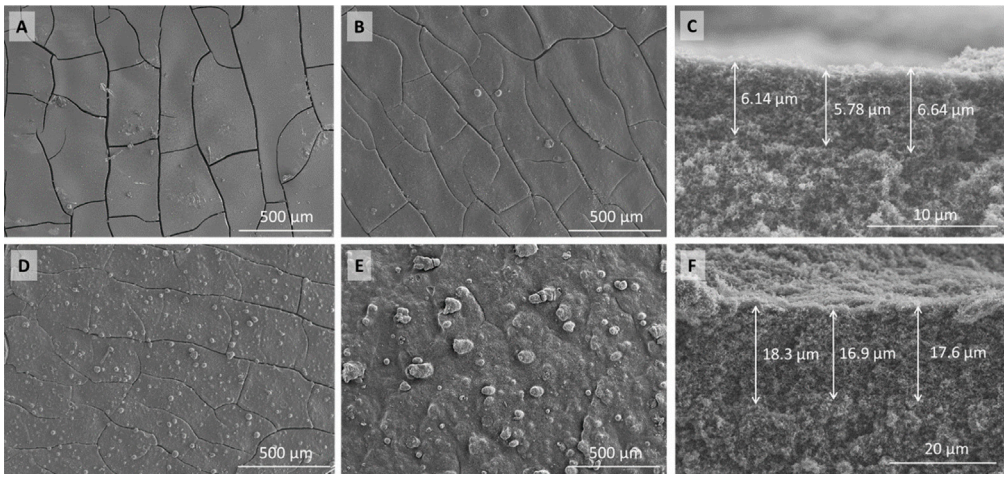

Fig. 3. Field emission scanning electron microscopy (FESEM) images of pristine GDE (A), GDE coated with 0.46 mg cm^{-2} CB-1h (B), the cross-section of the GDE with 0.46 mg cm^{-2} CB-1h (C), GDE coated with 0.46 mg cm^{-2} CB-7.5h (D), and GDE coated 2 mg cm^{-2} CB-1h (E) and its cross-section (F).

literature [64]. However, further extension of acid-treatment time leads to a decline in oxygen content, amounting to 16.5 ± 2.0 wt% (CB-4h) and 10.4 ± 1.3 wt% (CB-7.5h). Compared to O and C contents, the share of H and N remains below 0.2 wt% for all CBs.

The decline in oxygen content for prolonged acid treatment durations (≥4 h) could be attributed to the desorption or decomposition of previously incorporated oxygen functional groups and carbon erosion under harshly acidic conditions [65–67]. Table S1 represents the BET surface area and pore volume of pristine and acid-treated CBs. The BET surface area slightly decreases from 213 m^2 g^{-1} for CB-0h to 195 m^2 g^{-1} and 200 m^2 g^{-1} for CB-1h and CB-2h, respectively; followed by a sharp drop to 133 m^2 g^{-1} for CB-4h. However, a longer acid treatment duration of 7.5 h leads to an increase in BET surface area from 133 m^2 g^{-1} to 171 m^2 g^{-1} due to an increased micropore area (Table S1). Activation processes, e.g., acid treatment, generally lead to defect formation due to carbon erosion and increased specific surface area, particularly for carbons with a less defective surface, such as graphite and solid carbon particles. In this work, the pristine CB is porous with the highest micropore area of 70 m^2 g^{-1} (Table S1), and further defect formation during acid treatment can cause two effects. First, it can increase the pore volume by further oxidizing the pore walls of porous carbon. Second, excessive defect formation may lead to the collapse of pore structures, leading to smaller pore volume and specific surface area [53].

Based on Table S1, the pore volume increases from 0.16 cm^3 g^{-1} for CB-0h to 0.26 cm^3 g^{-1} for CB-1h and 0.3 cm^3 g^{-1} for CB-2h, respectively, which implies the enlargement of pores during short acid treatment times. Subsequently, the total pore volume decreases to 0.22 cm^3 g^{-1} for CB-4h, which can be associated with the collapse of porous structure for prolonged acid treatment. The decline in total pore volume aligns with the significant drop in oxygen content (Fig. 2).

Additionally, Fig. S12 represents the XPS data for CB-0h, CB-1h, and CB-7.5h concerning their O1s and C1s spectra. CB-0h represents two separate peaks at 531.8 eV and 533.4 eV, which can be attributed to oxygen functional groups of C=O and O−C=O; respectively [38] In contrast, acid-treated CBs (CB-1h and CB-7.5h) only show one peak at 531.8 eV, which has been reported as the most active oxygen functional group for two-electron ORR [68]. Additionally, the C1s spectra display four distinct peaks for CB-0h at 284.8 eV, 286.1 eV, 287.5 eV, and 289.3 eV, which are associated to C−C, C−O, C=O, and O−C=O, respectively [38] Nonetheless, CB-1h and CB-7.5h show only two distinct peaks at 284.8 eV and 286.1 eV that could be related to the oxidation of carbon under acid treatment.

Fig. 3 presents the FESEM images of the as-prepared GDE electrodes with CB-1h and CB-7.5h at various loadings. The pristine GDE, without any catalyst coating on the GDL layer, displays a complex network of cracks, varying in width and length and forming a mosaic of irregular patterns (Fig. 3A). Coating the GDL with a catalyst layer covers the surface smoothly, partially filling the cracks (Fig. 3B &D). Interestingly, CB-1h (Fig. 3B) resulted in fewer agglomerates while air-brushing compared to CB-7.5h (Fig. 3D), which could be attributed to their different surface properties due to the higher acid-treatment residence time for CB-7.5h. In the case of 0.46 mg cm^{-2} loading, the catalyst layer amounts to 6.2 ± 0.4 µm (Fig. 3C), which increases to 17.6 ± 0.7 µm at a higher catalyst loading of 2 mg cm^{-2} (Fig. 3F). Additionally, at 2 mg cm^{-2} catalyst loading, the cracks are completely clogged, and larger agglomerates can be discerned (Fig. 3E). According to Fig. S2, all unused GDEs with and without catalysts represent a hydrophobic surface with a contact angle above 130°.

3.2. Effect of acid treatment on H_2O_2 production

Screening experiments (Fig. S3) using as-received commercial GDLs without coating any catalysts shows an increase in H_2O_2 concentration from 0.06 g L^{-1} to 5.3 g L^{-1} (catholyte volume of 100 mL) by increasing the current density from 5 mA cm^{-2} to 65 mA cm^{-2}, corresponding to a specific H_2O_2 production rate of 2.3 ± 0.1 mg cm^{-2} h^{-1} to 21.4 ± 5.5 mg cm^{-2} h^{-1}, respectively. In contrast, the current efficiency declines from 71 ± 2% at 5 mA cm^{-2} to 49 ± 12% at 65 mA cm^{-2}. This decline can be attributed to an enhanced cathode (pristine GDL) wettability at higher current densities due to electro-wetting, which can shift the three-phase boundary toward the gas channel due to electrolyte ingress [69]. Hence, the diffusion path for the formed H_2O_2 toward the bulk solution increases, promoting further electro-reduction of H_2O_2 to water (Eq. (2)) while diffusing through the microporous layer (≈ 60 µm, Fig. S10) of the electrode [18,70,71].

Fig. 4 depicts H_2O_2 concentration and the corresponding FE values over time for GDEs airbrushed with 0.46 mg cm^{-2} acid-treated CB catalysts. Accordingly, the H_2O_2 concentration reaches 4.0 ± 0.1 g L^{-1}, 2.7 ± 0.6 g L^{-1}, 1.9 ± 0.7 g L^{-1}, 2.4 ± 0.3 g L^{-1}, and 2.1 ± 0.2 g L^{-1} for CB-1h, CB-2h, CB-4h, and CB-7.5h, respectively. Compared to the pristine GDL, adding CB-1h as the catalyst enhances the specific H_2O_2 production rate by 50% to 32 mg cm^{-2} h^{-1}. Additionally, CB-1h shows the highest selectivity among all catalysts, with FE values above 80% over electrolysis time (Fig. 4B), which could be associated with its oxygen content (Fig. 2).

Except for CB-4h with an impaired FE from the beginning that can be attributed to its low oxygen content (Fig. 2) and BET surface area (Table S1), CB-2h and CB-7.5h represent FE values above 80% for the first 5 min and 10 min of electrolysis, declining to 51 ± 12% and 45 ± 6%

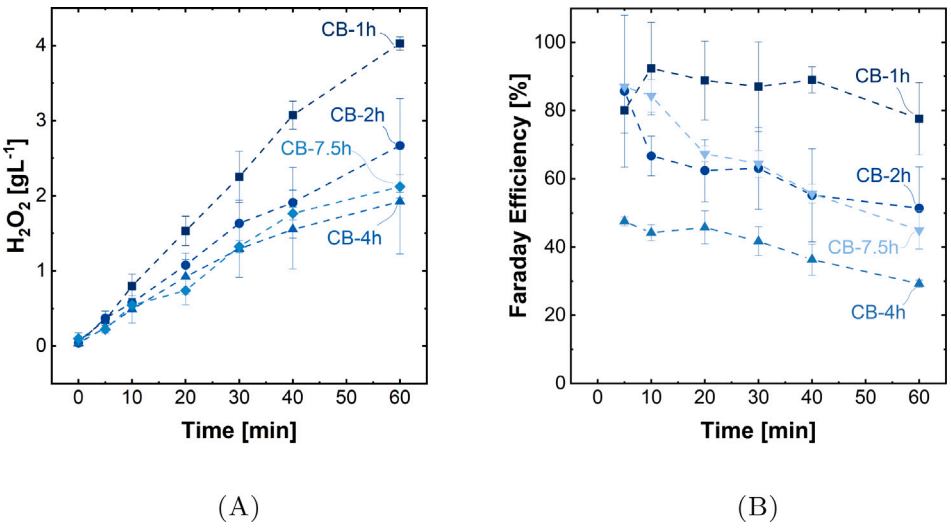

Fig. 4. Electro-generation of H_2O_2 (A) and the corresponding current efficiency (B) over time at 65 mA cm^{-2} using CB-1h, CB-2h, CB-4h, and CB-7.5-h. 200 mL of 0.1 M Na_2SO_4 and 0.5 M H_2SO_4 was circulated at 200 mL min^{-1} as catholyte and anolyte, respectively.

at t = 60 min, respectively. A similar, but not as pronounced, decline can be observed for CB-1h: a drop in FE value from 89 ± 4% at 40 min to 76 ± 11% at 60 min. One possible reason for these declines can be the gradual reduction of oxygen functional groups over electrolysis time [72]; however, the EA and FTIR analysis of fresh and used CB-1h catalyst indicates no decrease in oxygen content and functional groups (Fig. S13) after one-hour electrolysis. Another plausible explanation can be associated with the changes in surface properties of GDEs coated with these catalysts, e.g., hydrophilicity. A more hydrophilic GDE surface may cause a faster electrolyte ingress, moving the three-phase boundary toward the gas channel. Based on Fig. S2, GDEs coated with CB-2h and CB-7.5h represent the lowest contact angle of 133° and 142.5° among all unused GDEs.

$$O_{2(g)} + 2H^+ + 2e^- \longrightarrow H_2O_2,\ E^0 = 0.7\,V\ vs.\ RHE \quad (1)$$

$$H_2O_2 + 2H^+ + 2e^- \longrightarrow 2H_2O,\ E^0 = 1.76\,V\ vs.\ RHE \quad (2)$$

$$2H^+ + 2e^- \longrightarrow H_{2(g)},\ E^0 = 0.0\,V\ vs.\ RHE \quad (3)$$

Additionally, monitored cathodic potential (without ohmic drop (IR) correction) and cell potential over time depict a seamless behavior (Fig. S4), ranging from 0.17 V to 0.35 V vs. RHE and from 3.8 V to 4.5 V, respectively, which evidences the occurrence of no major parasitic reaction such as hydrogen evolution reaction (HER, Eq. (3)). pH and temperature profiles also indicate no abrupt changes over time, decreasing from 2.7 to 1.8 ± 0.1 and increasing from 21 °C to 23 °C, respectively (Fig. S4).

3.3. Effect of current density on H_2O_2 production

Increasing current density is required for high rates of H_2O_2 electro-generation. However, only few studies show on current densities above 100 mA cm^{-2} [53,56,58], while most studies are below this threshold [37,42–49,54,55,57,73]. Fig. 5 depicts H_2O_2 concentration (A) and current efficiency (B) over 60 min electrolysis at current densities of 100 mA cm^{-2} and 120 mA cm^{-2} next to 65 mA cm^{-2} for comparison.

Increase of current density from 65 mA cm^{-2} to 100 mA cm^{-2} boosts the electro-generation of H_2O_2, attaining a concentration of 6.6 ± 0.5 g L^{-1} after 60 min while maintaining FE values above 79% over the experiment time (Fig. 5). Nonetheless, further increasing of current density to 120 mA cm^{-2}, despite resulting in a slightly higher initial H_2O_2 concentration of 1.2 ± 0.4 g L^{-1} at t = 5 min compared to that (0.9 g L^{-1}) at 100 mA cm^{-2}, shows a severe drop in H_2O_2 production rate, particularly after 30 min, and amounts to a final value of 5.5 ± 0.2 g L^{-1}. Correspondingly, the FE values stay above 80% at 120 mA cm^{-2} over the first 30 min, followed by a significant decline to 55% over the rest of experiment (Fig. 5B).

Based on Fig. S5, the cell potential slightly increases from 5.00 ± 0.13 V to 5.7 ± 0.1 V at 100 mA cm^{-2}, while it rises more drastically from 6.00 ± 0.13 V to 7.2 ± 0.5 V at 120 mA cm^{-2}. This increase in cell potential at higher current density could be associated with the counter electrode potential on which oxygen evolution reaction (OER) occurs. The formation of bubbles on the counter electrode impairs the contact between the electrolyte and electrode and increases ohmic resistance, causing a higher cell potential [74]. Additionally, the highest temperature increase was observed at 120 mA cm^{-2}, from 21 °C to 29 °C (Fig. S5D).

However, increasing current density has no significant influence on the recorded cathodic potential (without ohmic drop (IR) correction), varying from 0.26 ± 0.02 V to 0.31 ± 0.04 V vs. RHE for 100 mA cm^{-2} and from 0.28 ± 0.01 V to 0.33 ± 0.01 V vs. RHE for 120 mA cm^{-2} (Fig. S5A). For comparison reasons, monitored cathodic and cell potentials at 120 mA cm^{-2} is plotted once N_2 was fed into the GDE and HER occurred at the lack of O_2, showing a more negative value of −0.38 V vs. RHE and 8.5 V, respectively. This comparison indicates that HER as a parasitic reaction holds an insignificant contribution during electrolysis at 120 mA cm^{-2}, particularly after the first 30 min. Hence, one credible explanation for the steep decline in H_2O_2 production and FE originates from the slow back diffusion of formed H_2O_2 toward the bulk solution as electrolyte ingresses into the GDE pore network over time, enhancing its further electro-reduction to water (Eq. (2)) [18,61,70,71]. Furthermore, this electrolyte ingress or electrode wetting, promoted at higher current densities, could also shift the three-phase boundary to the MPL instead of the CL, decreasing the selectivity of GDE due to the lack of catalysts.

Fig. 6 illustrates the H_2O_2 concentration and FE for GDEs with a higher catalyst loading of 0.86 mg cm^{-2} and 2 mg cm^{-2} at 120 mA cm^{-2}. Accordingly, the increase of CL thickness (Fig. 3) led to a linear increase of H_2O_2 concentration over the course of the experiment, amounting to 8.0 ± 0.3 g L^{-1} and 8.9 ± 0.3 g L^{-1} for GDEs with 0.86 mg cm^{-2} and 2 mg cm^{-2} loadings, respectively; compared to 5.5 ± 0.2 g L^{-1} achieved for the GDE with 0.46 mg cm^{-2} catalyst loading. Additionally, the FE stays above 80% throughout the electrolysis, with a value of 81 ± 3% for 0.86 mg cm^{-2} and 89 ± 3% for 2 mg cm^{-2} at 60 min.

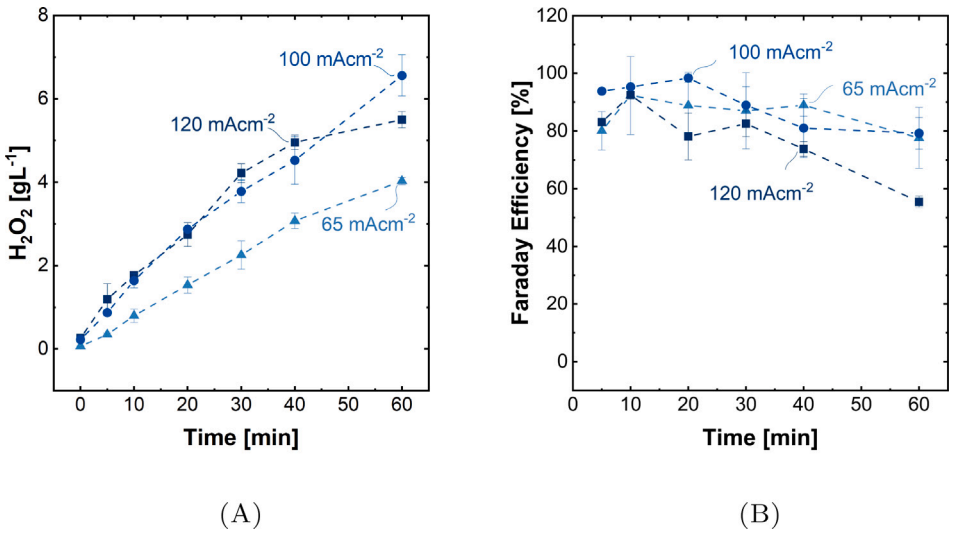

Fig. 5. Electro-generation of H_2O_2 (A) and the corresponding current efficiency (B) over time using CB-1h as the catalyst at higher current densities. 200 mL of 0.1 M Na_2SO_4 and 0.5 M H_2SO_4 was circulated at 200 mL min^{-1} as catholyte and anolyte, respectively.

A higher catalyst loading increases the CL's thickness and better fills the intrinsic cracks of the pristine GDE (Fig. 3). However, the contact angle slightly increases from 157.4° for 0.46 mg cm^{-2} to 163° for 2 mg cm^{-2}. Considering similar hydrophobic features of GDEs with different loadings at the same applied current density, a similar wetting behavior (electrolyte ingress) for GDEs is expected. Therefore, it can be implied that the higher catalyst loading contributes to holding the three-phase boundary within an extended CL, maintaining a linear H_2O_2 production rate and FEs above 80% over the course of the experiments. These results highlight the importance of positioning the three-phase boundary within the CL over electrolysis time since a lack of catalyst can significantly decline process efficiency.

Fig. S6 compares the H_2O_2 production and FE for the GDE coated with CB-1h to those for the GDE coated with as-received CB catalysts, without any acid-treatment (CB-0h) at 120 mA cm^{-2}. Evidently, the GDE coated with CB-0h represents an inferior performance, with an initial FE of 63 ± 3% dropping to 39% at t = 60 min, which can be attributed to the lack of oxygen content (Fig. 2).

3.4. Long-term experiments

Although the increase of catalyst content enhanced the electro-generation of H_2O_2 over one-hour electrolysis, the functionality of as-fabricated GDEs for a longer electrolysis time remains unclear. Thereby, the GDE with the highest catalyst loading of 2 mg cm^{-2} was tested over 450 min of electrolysis using CB-1h, and the data are presented in Fig. 7.

Based on Fig. 7A, the concentration of H_2O_2 linearly rises up to 7.9 g L^{-1} over the first 60 min, followed by a slower increase to 14.9 g L^{-1} over the next 150 min (t_{exp} = 210 min), when it reaches a plateau over the rest of electrolysis. Consequently, the FE severely declined from 78 ± 7 at 60 min to 19% at 450 min. Since monitored cathodic and cell potentials show no abrupt change over the course of the experiment (Fig. S7), it can be concluded that the contribution of the parasitic HER reaction (Eq. (3)) on declining the FE values remains insignificant. Additionally, the EA and FTIR analyses of the fresh and used GDEs after 450 min of electrolysis show no significant decline in oxygen content and oxygen functional groups (Fig. S13) due to their possible gradual

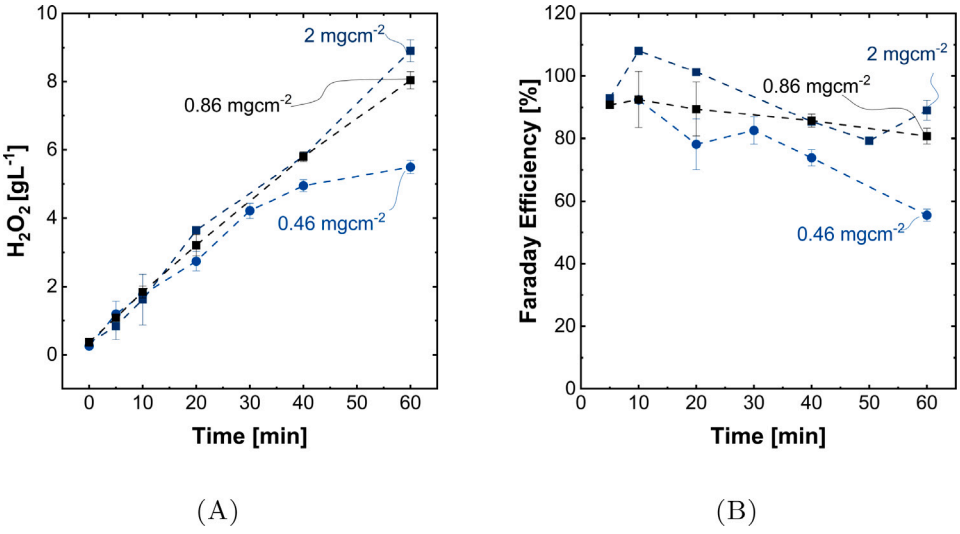

Fig. 6. Electro-generation of H_2O_2 (A) and the corresponding current efficiency (B) over time using CB-1h with two different catalyst loading of 0.46 mg cm^{-2} and 2 mg cm^{-2} at 120 mA cm^{-2}. 200 mL of 0.1 M Na_2SO_4 and 0.5 M H_2SO_4 was circulated at 200 mL min^{-1} as catholyte and anolyte, respectively.

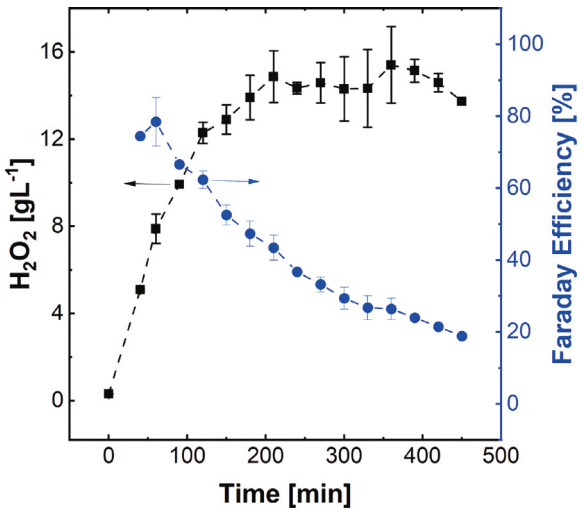

Fig. 7. Electro-generation of H_2O_2 and the corresponding current efficiency over 450 min electrolysis using CB-1h with a catalyst loading of 2 mg cm^{-2} at 120 mA cm^{-2}. 200 mL of 0.1 M Na_2SO_4 and 0.5 M H_2SO_4 was circulated at 200 mL min^{-1} as catholyte and anolyte, respectively.

reduction during electrolysis [72], which shows the stability of oxygen functional groups overtime at 120 mA cm^{-2}.

Similar to one-hour electrolysis using GDE with 0.46 mg cm^{-2} loading, electrolyte ingress over time and pushing the position of the three-phase boundary to the MPL, where no catalyst is present, can explain the impaired functionality of the GDE after 60 min since it promotes further electro-reduction of formed H_2O_2 (Eq. (2)) inside the porous network of GDEs instead diffusing back to the bulk solution [18,61,70,71]. Additionally, shifting the three-phase boundary to the vicinity of the gas channel enhances the vaporization and dripping of the catholyte to the O_2 gas stream, where it is carried away to the water trap and further is released to the off-gas duct (Fig. 1). Recently, our group has reported on electrolyte permeation to the gas channel during CO_2 electrolysis at current densities above 100 mA cm^{-2}, which contained a higher ion concentration compared to the bulk catholyte that indicates high local concentrations in the vicinity of the catalyst layer [75].

Analysis of the samples from the water trap beaker, placed at the outlet of the O_2 gas channel (Fig. 1), reveals a drastic increase in Na^+ concentration from below 0.18 g L^{-1} over the first 180 min to 3.7 ± 0.4 g L^{-1} at t = 450 min (Fig. S8A). Similarly, no H_2O_2 was detected in the water trap solution during the first 180 min, while it increased to 2 g L^{-1} over the rest of the experiment (Fig. S8B) It should be noted that 2 g L^{-1} of H_2O_2 implies a higher local H_2O_2 concentration in the permeated catholyte since the water trap was filled with 20 mL DI water in the beginning (Fig. S8B).

Furthermore, FESEM analysis and EDX mapping of the backside of the used GDE after 450 min of electrolysis (Fig. S9) indicate the presence of Na-containing salt crystals, proving the electrolyte ingress into the gas channel side over the long-term experiment. Moreover, characterization of used GDEs after electrolysis experiments (Fig. S10 & Fig. S11) illustrates the deposition of Na^+ salt layer on the top of the CL, increasing the thickness of the CL by several micrometers (Fig. S11). The contact angle of the used GDE after the long-term experiments severely drops from 163° to 48.7° (Fig. S2), representing a hydrophilic surface, which can be attributed to the deposition of Na^+ salts (Fig. S10). Therefore, the characterization of GDEs can be severely altered by electrolysis experiments, particularly longer runs, which must be considered while optimizing GDE fabrication parameters.

Table S2 collects the specific H_2O_2 production rates, FE values, and experimental conditions from this work and compares them with the literature [39,42,44,46–49,53–56,58,59,76–78]. For instance, Zhang and co-workers [56] have reported the highest value of 283 mg cm^{-2} at 400 mA cm^{-2} with an FE of 90% using reduced graphene oxide, which reduced to 51 mg cm^{-2} at a lower current density of 100 mA cm^{-2} with 87% FE. However, changing the catalyst to CB lowered the production rate to 44.2 mg cm^{-2} at 100 mA cm^{-2} [56]. In comparison, a specific H_2O_2 production rate of 52.5 mg cm^{-2} with an FE of 89% was attained in this work at 100 mA cm^{-2}, increasing to 63.1 mg cm^{-2} and 64.3 mg cm^{-2} at the maximum applied current density of 120 mA cm^{-2} for CB-1h with higher catalyst loadings (Fig. 6).

4. Conclusion

This study investigated the electro-generation of H_2O_2 in a flow-through module using GDEs, with a relatively large geometrical surface area (e.g., 25 cm^2) compared to the literature. These GDEs were coated with acid-treated carbon black (CB) catalysts. Elemental analysis of CB catalysts revealed that oxygen content in CB catalysts increased after acid treatment durations of 1 h and 2 h but declined with longer durations of 4 h and 7.5 h, which can be associated to erosion of carbon or the desorption of oxygen functional groups over extended times. Electrochemical experiments at 65 mA cm^{-2} demonstrated the superiority of catalysts with high oxygen content (CB-1h and CB-2h) and BET surface area (CB-1h, CB-2h, and CB-7.5h). Despite the initial high Faraday efficiency (FE) of GDEs (≥80%), their performance declined overtime for both short-term (60 min) and long-term (450 min) experiments. Surface characterization of fresh and used GDEs indicated that decreasing hydrophobicity over time, especially at higher current densities (e.g., 120 mA cm^{-2}) contributes to the observed decline in FE since no significant decline in oxygen content and functional groups of GDEs after usage was observed. These results highlight the importance of maintaining GDEs' hydrophobic properties during electrolysis, particularly over long-term runs at industry-relevant current densities (≥100 mA cm^{-2}), which must be addressed for electrochemical H_2O_2 generation as a sustainable, decentralized alternative to the traditional anthraquinone process.

CRediT authorship contribution statement

Mojtaba Mohseni: Writing – original draft, Visualization, Supervision, Project administration, Methodology, Investigation, Formal analysis, Conceptualization. **Waralee Dilokekunakul:** Writing – original draft, Visualization, Validation, Supervision, Methodology, Investigation, Formal analysis. **Matthias Wessling:** Writing – review & editing, Supervision, Resources, Funding acquisition, Conceptualization. **Robert G. Keller:** Writing – review & editing, Validation, Supervision, Project administration, Funding acquisition, Formal analysis, Conceptualization.

Declaration of competing interest

The authors declare that they have no known competing financial interests or personal relationships that could have appeared to influence the work reported in this paper.

Data availability

Data will be made available on request.

Acknowledgments

This work was supported by the German Federal Ministry of Education and Research (BMBF) under the project "HyInnoChem" (03ZU1115I) within the framework of the H_2-cluster. This work was conducted in part at the Competence Center for Industrial Electrochemistry ELECTRA, which is supported by the European Regional Development Fund (ERDF) and the Federal State of North Rhine-Westphalia (grant no. ERDF 05 00 07 7). The authors thank Jacqueline Kieven, Timo Linzenmeier, Justin Gottfried, and Karin Faensen for their support and contributions.

Appendix A. Supplementary data

Supplementary material related to this article can be found online at https://doi.org/10.1016/j.electacta.2024.144533.

References

[1] B.O. Burek, S. Bormann, F. Hollmann, J.Z. Bloh, D. Holtmann, Hydrogen peroxide driven biocatalysis, Green Chem. 21 (2019) 3232–3249.

[2] M.M. Heravi, N. Ghalavand, E. Hashemi, Hydrogen peroxide as a green oxidant for the selective catalytic oxidation of benzylic and heterocyclic alcohols in different media: An overview, Chemistry 2 (1) (2020) 101–178.

[3] K.L. Ortega, B. Rech, A.L. Ferreira Costa, M. Perez Sayans, P.H. Braz-Silva, Is 0.5% hydrogen peroxide effective against SARS-CoV-2? Oral Dis. 28 (S1) (2022) 937–939.

[4] T. Pottage, I. Garratt, O. Onianwa, J. Carter, A. Bennett, Rapid inactivation of SARS-CoV-2 after exposure to vapour hydrogen peroxide, J. Hosp. Infect. 118 (2021) 77–78.

[5] W. Kopacz, A. Okninski, A. Kasztankiewicz, P. Nowakowski, G. Rarata, P. Maksimowski, Hydrogen peroxide – A promising oxidizer for rocket propulsion and its application in solid rocket propellants, FirePhysChem 2 (1) (2022) 56–66.

[6] S. Li, J. Ma, F. Xu, L. Wei, D. He, Fundamental principles and environmental applications of electrochemical hydrogen peroxide production: A review, Chem. Eng. J. 452 (2023) 139371.

[7] J. García-Serna, T. Moreno, P. Biasi, M.J. Cocero, J.-P. Mikkola, T.O. Salmi, Engineering in direct synthesis of hydrogen peroxide: targets, reactors and guidelines for operational conditions, Green Chem. 16 (2014) 2320–2343.

[8] R. Ciriminna, L. Albanese, F. Meneguzzo, M. Pagliaro, Hydrogen peroxide: A key chemical for today's sustainable development, ChemSusChem 9 (24) (2016) 3374–3381.

[9] J.M. Campos-Martin, G. Blanco-Brieva, J.L.G. Fierro, Hydrogen peroxide synthesis: An outlook beyond the anthraquinone process, Angew. Chem. Int. Ed. 45 (42) (2006) 6962–6984.

[10] J.H. Lunsford, The direct formation of H_2O_2 from H_2 and O_2 over palladium catalysts, J. Catal. 216 (1) (2003) 455–460, 40th Anniversary Commemorative Issue.

[11] J.K. Edwards, S.J. Freakley, R.J. Lewis, J.C. Pritchard, G.J. Hutchings, Advances in the direct synthesis of hydrogen peroxide from hydrogen and oxygen, Catal. Today 248 (2015) 3–9, Perspectives in the H_2O_2 direct synthesis reaction process.

[12] Y. Jiang, P. Ni, C. Chen, Y. Lu, P. Yang, B. Kong, A. Fisher, X. Wang, Selective electrochemical H_2O_2 production through two-electron oxygen electrochemistry, Adv. Energy Mater. 8 (31) (2018) 1801909.

[13] M.N. Young, M.J. Links, S.C. Popat, B.E. Rittmann, C.I. Torres, Tailoring microbial electrochemical cells for production of hydrogen peroxide at high concentrations and efficiencies, ChemSusChem 9 (23) (2016) 3345–3352.

[14] E.C. Murphy, A.J. Friedman, Hydrogen peroxide and cutaneous biology: Translational applications, benefits, and risks, J. Am. Acad. Dermatol. 81 (6) (2019) 1379–1386.

[15] N. Oturan, M.A. Oturan, Electro-fenton process: Background, new developments, and applications, in: Electrochemical Water and Wastewater Treatment, Elsevier, 2018, pp. 193–221.

[16] Y. Liu, Y. Zhao, J. Wang, Fenton/fenton-like processes with in-situ production of hydrogen peroxide/hydroxyl radical for degradation of emerging contaminants: Advances and prospects, J. Hazard. Mater. 404 (2021) 124191.

[17] W. Zhou, X. Meng, J. Gao, A.N. Alshawabkeh, Hydrogen peroxide generation from O_2 electroreduction for environmental remediation: A state-of-the-art review, Chemosphere 225 (2019) 588–607.

[18] M. Mohseni, D. Felder, K. Percin, M. Thönes, M. Gassenmeier, R. Kupec, C. Weidlich, J. Linkhorst, R.G. Keller, M. Wessling, Toward decentralized wastewater treatment: A flow-through module using microtubular gas diffusion electrodes for micropollutants removal, J. Hazard. Mater. 458 (2023) 131987.

[19] Y. Tian, D. Deng, L. Xu, H. Li, Z. Wu, S. Zhang, Strategies for sustainable production of hydrogen peroxide via oxygen reduction reaction: From catalyst design to device setup, Nano-Micro Lett. 15 (122) (2023).

[20] S. Anantharaj, S. Pitchaimuthu, S. Noda, A review on recent developments in electrochemical hydrogen peroxide synthesis with a critical assessment of perspectives and strategies, Adv. Colloid Interface Sci. 287 (2021) 102331.

[21] Q. Cui, D.J. Bell, S. Wang, M. Mohseni, D. Felder, J. Lölsberg, M. Wessling, Wet-spun PEDOT/CNT composite hollow fibers as flexible electrodes for H_2O_2 production, ChemElectroChem 8 (9) (2021) 1665–1673.

[22] S. Siahrostami, A. Verdaguer-Casadevall, M. Karamad, D. Deiana, P. Malacrida, B. Wickman, M. Escudero-Escribano, E.A. Paoli, R. Frydendal, T.W. Hansen, I. Chorkendorff, I.E.L. Stephens, J. Rossmeisl, Enabling direct H_2O_2 production through rational electrocatalyst design, Nature Mater. 12 (2013) 1137–1143.

[23] J. Gao, B. Liu, Progress of electrochemical hydrogen peroxide synthesis over single atom catalysts, ACS Mater. Lett. 2 (8) (2020) 1008–1024.

[24] Q. Zhang, Y. Chen, J. Pan, R. Daiyan, E.C. Lovell, J. Yun, R. Amal, X. Lu, Electrosynthesis of hydrogen peroxide through selective oxygen reduction: A carbon innovation from active site engineering to device design, Small 19 (40) (2023) 2302338.

[25] H.W. Kim, M.B. Ross, N. Kornienko, L. Zhang, J. Guo, P. Yang, B.D. McCloskey, Efficient hydrogen peroxide generation using reduced graphene oxide-based oxygen reduction electrocatalysts, Nat. Catal. 1 (4) (2018) 282–290.

[26] Y.J. Sa, J.H. Kim, S.H. Joo, Active edge-site-rich carbon nanocatalysts with enhanced electron transfer for efficient electrochemical hydrogen peroxide production, Angew. Chem. Int. Ed. 58 (4) (2019) 1100–1105.

[27] Y. Liu, X. Quan, X. Fan, H. Wang, S. Chen, High-yield electrosynthesis of hydrogen peroxide from oxygen reduction by hierarchically porous carbon, Angew. Chem. Int. Ed. 54 (23) (2015) 6837–6841.

[28] M. Neergat, V. Gunasekar, R. Singh, Oxygen reduction reaction and peroxide generation on Ir, Rh, and their selenides–A comparison with Pt and RuSe, J. Electrochem. Soc. 158 (9) (2011) B1060.

[29] R. Rahul, R. Singh, B. Bera, R. Devivaraprasad, M. Neergat, The role of surface oxygenated-species and adsorbed hydrogen in the oxygen reduction reaction (ORR) mechanism and product selectivity on Pd-based catalysts in acid media, Phys. Chem. Chem. Phys. 17 (23) (2015) 15146–15155.

[30] R. Das, D. Choudhury, R. Maurya, S. Sharma, M. Neergat, Influence of nitrogen doping into carbon on the activation barrier of ORR in alkaline medium: An investigation based on eyring analysis, Langmuir 39 (12) (2023) 4351–4361.

[31] M. Carmo, M. Linardi, J.G. Rocha Poco, H_2O_2 Treated carbon black as electrocatalyst support for polymer electrolyte membrane fuel cell applications, Int. J. Hydrog. Energy 33 (21) (2008) 6289–6297.

[32] J. yi Chen, N. Li, L. Zhao, Three-dimensional electrode microbial fuel cell for hydrogen peroxide synthesis coupled to wastewater treatment, J. Power Sources 254 (2014) 316–322.

[33] R.A. Rozendal, E. Leone, J. Keller, K. Rabaey, Efficient hydrogen peroxide generation from organic matter in a bioelectrochemical system, Electrochem. Commun. 11 (9) (2009) 1752–1755.

[34] W. Li, J. Liu, C. Yan, The electrochemical catalytic activity of single-walled carbon nanotubes towards VO^{2+}/VO^{2+} and V^{3+}/V^{2+} redox pairs for an all vanadium redox flow battery, Electrochim. Acta 79 (2012) 102–108.

[35] Y. Ding, W. Zhou, J. Gao, F. Sun, G. Zhao, H_2O_2 Electrogeneration from O_2 electroreduction by N-doped carbon materials: A mini-review on preparation methods, selectivity of N sites, and prospects, Adv. Mater. Interfaces 8 (10) (2021) 2002091.

[36] H. He, S. Liu, Y. Liu, L. Zhou, H. Wen, R. Shen, H. Zhang, X. Guo, J. Jiang, B. Li, Review and perspectives on carbon-based electrocatalysts for the production of H_2O_2 via two-electron oxygen reduction, Green Chem. 25 (2023) 9501–9542.

[37] S. Chen, Z. Chen, S. Siahrostami, T.R. Kim, D. Nordlund, D. Sokaras, S. Nowak, J.W.F. To, D. Higgins, R. Sinclair, J.K. Nørskov, T.F. Jaramillo, Z. Bao, Defective carbon-based materials for the electrochemical synthesis of hydrogen peroxide, ACS Sustain. Chem. Eng. 6 (1) (2018) 311–317.

[38] M. Assumpção, R. De Souza, D. Rascio, J. Silva, M.L. Calegaro, I. Gaubeur, T.R.L.C.d. Paixão, P. Hammer, M. Lanza, M.C.d. Santos, A comparative study of the electrogeneration of hydrogen peroxide using vulcan and printex carbon supports, Carbon 49 (8) (2011) 2842–2851.

[39] H. Luo, C. Li, C. Wu, X. Dong, In situ electrosynthesis of hydrogen peroxide with an improved gas diffusion cathode by rolling carbon black and PTFE, RSC Adv. 5 (80) (2015) 65227–65235.

[40] P.J.M. Cordeiro-Junior, M.S. Kronka, L.A. Goulart, N.C. Veríssimo, L.H. Mascaro, M.C. dos Santos, R. Bertazzoli, M.R. de Vasconcelos Lanza, Catalysis of oxygen reduction reaction for H_2O_2 electrogeneration: The impact of different conductive carbon matrices and their physicochemical properties, J. Catal. 392 (2020) 56–68.

[41] A. Loh, D.P. Trudgeon, X. Li, M.-C. Liu, L.-B. Kong, F.C. Walsh, Selection of oxygen reduction catalysts for secondary tri-electrode zinc–air batteries, Sci. Rep. 12 (1) (2022) 6696.

[42] C. Li, C. Hu, Y. Song, Y.-M. Sun, W. Yang, M. Ma, Active oxygen functional group modification and the combined interface engineering strategy for efficient hydrogen peroxide electrosynthesis, ACS Appl. Mater. Interfaces 14 (41) (2022) 46695–46707.

[43] X. Yu, M. Zhou, G. Ren, L. Ma, A novel dual gas diffusion electrodes system for efficient hydrogen peroxide generation used in electro-fenton, Chem. Eng. J. 263 (2015) 92–100.

[44] N. Li, J. An, L. Zhou, T. Li, J. Li, C. Feng, X. Wang, A novel carbon black graphite hybrid air-cathode for efficient hydrogen peroxide production in bioelectrochemical systems, J. Power Sources 306 (2016) 495–502.

[45] M. Panizza, G. Cerisola, Electrochemical generation of H_2O_2 in low ionic strength media on gas diffusion cathode fed with air, Electrochim. Acta 54 (2) (2008) 876–878.

[46] J. Lu, X. Liu, Q. Chen, J. Zhou, Coupling effect of nitrogen-doped carbon black and carbon nanotube in assembly gas diffusion electrode for H_2O_2 electrogeneration and recalcitrant pollutant degradation, Sep. Purif. Technol. 265 (2021) 118493.

[47] G. Daniel, Y. Zhang, S. Lanzalaco, F. Brombin, T. Kosmala, G. Granozzi, A. Wang, E. Brillas, I. Sirés, C. Durante, Chitosan-derived nitrogen-doped carbon electrocatalyst for a sustainable upgrade of oxygen reduction to hydrogen peroxide in UV-assisted electro-fenton water treatment, ACS Sustain. Chem. Eng. 8 (38) (2020) 14425–14440.
[48] J. An, N. Li, Q. Zhao, Y. Qiao, S. Wang, C. Liao, L. Zhou, T. Li, X. Wang, Y. Feng, Highly efficient electro-generation of H_2O_2 by adjusting liquid-gas-solid three phase interfaces of porous carbonaceous cathode during oxygen reduction reaction, Water Res. 164 (2019) 114933.
[49] B. Garza-Campos, D. Morales-Acosta, A. Hernández-Ramírez, J. Guzmán-Mar, L. Hinojosa-Reyes, J. Manríquez, E. Ruiz-Ruiz, Air diffusion electrodes based on synthetized mesoporous carbon for application in amoxicillin degradation by electro-fenton and solar photo electro-fenton, Electrochim. Acta 269 (2018) 232–240.
[50] D. Iglesias, A. Giuliani, M. Melchionna, S. Marchesan, A. Criado, L. Nasi, M. Bevilacqua, C. Tavagnacco, F. Vizza, M. Prato, P. Fornasiero, N-doped graphitized carbon nanohorns as a forefront electrocatalyst in highly selective O_2 reduction to H_2O_2, Chem 4 (1) (2018) 106–123.
[51] C.H. Choi, M. Kim, S.J.C. Han Chang Kwon, H.-T.K. Seongho Yun, K.J.J. Mayrhofer, H. Kim, M. Choi, Tuning selectivity of electrochemical reactions by atomically dispersed platinum catalyst, Nature Commun. 7 (2016) 10922.
[52] K. Lee, J. Lim, M.J. Lee, K. Ryu, H. Lee, J.Y. Kim, H. Ju, H.-S. Cho, B.-H. Kim, M.C. Hatzell, J. Kang, S.W. Lee, Structure-controlled graphene electrocatalysts for high-performance H_2O_2 production, Energy Environ. Sci. 15 (2022) 2858–2866.
[53] C. Xia, Y. Xia, P. Zhu, L. Fan, H. Wang, Direct electrosynthesis of pure aqueous H_2O_2 solutions up to 20% by weight using a solid electrolyte, Science 366 (6462) (2019) 226–231.
[54] Y. Sheng, Y. Zhao, X. Wang, R. Wang, T. Tang, Electrogeneration of H_2O_2 on a composite acetylene black-PTFE cathode consisting of a sheet active core and a dampproof coating, Electrochim. Acta 133 (2014) 414–421.
[55] Y. Gu, S. Wu, Y. Cao, M. Liu, S. Chen, X. Quan, H. Yu, Construction of a microchannel aeration cathode for producing H_2O_2 via oxygen reduction reaction, ACS Appl. Mater. Interfaces 13 (47) (2021) 56045–56053.
[56] X. Zhang, X. Zhao, Z.A. Peng Zhu, Z.-Y. Wu, Y. Liu, H. Wang, Electrochemical oxygen reduction to hydrogen peroxide at practical rates in strong acidic media, Nat. Commun. Vol. 13 (2022) 2880.
[57] Z. Lu, G. Chen, S. Siahrostami, Z. Chen, K. Liu, J. Xie, L. Liao, T. Wu, D. Lin, Y. Liu, et al., High-efficiency oxygen reduction to hydrogen peroxide catalysed by oxidized carbon materials, Nat. Catal. 1 (2) (2018) 156–162.
[58] P.J.M. Cordeiro-Junior, J. Lobato Bajo, M. Lanza, M.A. Rodrigo Rodrigo, Highly efficient electrochemical production of hydrogen peroxide using the GDE technology, Ind. Eng. Chem. Res. 61 (30) (2022) 10660–10669.
[59] Q. Zhang, M. Zhou, G. Ren, Y. Li, Y. Li, X. Du, Highly efficient electrosynthesis of hydrogen peroxide on a superhydrophobic three-phase interface by natural air diffusion, Nat. Commun. 11 (1) (2020) 1731.
[60] N. Dhanda, Y.K. Panday, S. Kumar, Recent advances in the electrochemical production of hydrogen peroxide, Electrochim. Acta (2024) 143872.
[61] M. Mohseni, F. Voit, Y. Xie, K. Demeestere, G. Du Laing, S. Yüce, R. Keller, M. Wessling, Tubular and bio-based carbons as binder-free gas diffusion electrodes for heterogeneous electro-fenton to remove micropollutants, Electrochim. Acta (2024) 143755.
[62] M. Thommes, K. Kaneko, A.V. Neimark, J.P. Olivier, F. Rodriguez-Reinoso, J. Rouquerol, K.S. Sing, Physisorption of gases, with special reference to the evaluation of surface area and pore size distribution (IUPAC technical report), Pure Appl. Chem. 87 (9–10) (2015) 1051–1069.
[63] R.F.P. Nogueira, M.C. Oliveira, W.C. Paterlini, Simple and fast spectrophotometric determination of H_2O_2 in photo-fenton reactions using metavanadate, Talanta 66 (1) (2005) 86–91.
[64] J.-H. Kim, S.Y. Hwang, J.E. Park, G.B. Lee, H. Kim, S. Kim, B.U. Hong, Impact of the oxygen functional group of nitric acid-treated activated carbon on KOH activation reaction, Carbon Lett. 29 (2019) 281–287.
[65] J. He, H. Li, W. Yang, J. Lu, Y. Lu, T. Liu, S. Shi, Experimental study on erosion mechanism and pore structure evolution of bituminous and anthracite coal under matrix acidification and its significance to coalbed methane recovery, Energy 283 (2023) 128485.
[66] R.P. Rocha, M.F.R. Pereira, J.L. Figueiredo, Characterisation of the surface chemistry of carbon materials by temperature-programmed desorption: An assessment, Catal. Today (2023) 114136.
[67] G. Tremblay, F. Vastola, P. Walker Jr., Thermal desorption analysis of oxygen surface complexes on carbon, Carbon 16 (1) (1978) 35–39.
[68] L. Chu, Z. Sun, L. Cang, X. Wang, G. Fang, J. Gao, Identifying the roles of oxygen-containing functional groups in carbon materials for electrochemical synthesis of H_2O_2, J. Environ. Chem. Eng. 11 (3) (2023) 109826.
[69] A.M. Kalde, M. Grosseheide, S. Brosch, S.V. Pape, R.G. Keller, J. Linkhorst, M. Wessling, Micromodel of a gas diffusion electrode tracks in-operando pore-scale wetting phenomena, Small 18 (49) (2022) 2204012.
[70] W. Zhou, J. Gao, Y. Ding, H. Zhao, X. Meng, Y. Wang, K. Kou, Y. Xu, S. Wu, Y. Qin, Drastic enhancement of H_2O_2 electro-generation by pulsed current for ibuprofen degradation: Strategy based on decoupling study on H_2O_2 decomposition pathways, Chem. Eng. J. 338 (2018) 709–718.
[71] M. Mohseni, W. Zängler, K. Demeestere, G. Du Laing, S. Bhandari, A.K. Mechler, S. Yüce, R.G. Keller, M. Wessling, One-pot synthesized, Fe-incorporated self-standing carbons with a hierarchical porosity remove carbamazepine and sulfamethoxazole through heterogeneous electro-fenton, Chem. Eng. J. (2022) 137006.
[72] T. Kar, R. Devivaraprasad, B. Bera, R. Ramesh, M. Neergat, Investigation on the reduction of the oxides of Pd and graphite in alkaline medium and the simultaneous evolution of oxygen reduction reaction and peroxide generation features, Electrochim. Acta 191 (2016) 81–89.
[73] Q. Zhao, Y. Wang, W.-H. Lai, F. Xiao, Y. Lyu, C. Liao, M. Shao, Approaching a high-rate and sustainable production of hydrogen peroxide: oxygen reduction on Co-N-C single-atom electrocatalysts in simulated seawater, Energy Environ. Sci. 14 (2021) 5444–5456.
[74] X. Zhao, H. Ren, L. Luo, Gas bubbles in electrochemical gas evolution reactions, Langmuir 35 (16) (2019) 5392–5408.
[75] M. Wrobel, S. Kriescher, T. Schiffer, R. Keller, M. Wessling, On the weeping of the GDE cathode during bipolar membrane-based electrochemical CO_2 reduction reaction at high current densities, Chem. Eng. J. 474 (2023) 145335.
[76] V.B. Lima, L.A. Goulart, R.S. Rocha, J.R. Steter, M.R. Lanza, Degradation of antibiotic ciprofloxacin by different AOP systems using electrochemically generated hydrogen peroxide, Chemosphere 247 (2020) 125807.
[77] P.J.M. Cordeiro-Junior, C.S. Jiménez, M.R. de Vasconcelos Lanza, M.A.R. Rodrigo, Electrochemical production of extremely high concentrations of hydrogen peroxide in discontinuous processes, Sep. Purif. Technol. 300 (2022) 121847.
[78] W.R. Barros, T. Ereno, A.C. Tavares, M.R. Lanza, In situ electrochemical generation of hydrogen peroxide in alkaline aqueous solution by using an unmodified gas diffusion electrode, ChemElectroChem 2 (5) (2015) 714–719.